Hindawi
Mathematical Problems in Engineering
Volume 2019, Article ID 4153715, 12 pages
https://doi.org/10.1155/2019/4153715

Research Article

A Comprehensive Optimization Design Method of Aerodynamic, Acoustic, and Stealth of Helicopter Rotor Blades Based on Genetic Algorithm

Mingxu Yi,[1] Yalin Pan,[1] Jun Huang,[1] Lifeng Wang,[1] and Dawei Liu[2]

[1] *School of Aeronautic Science and Engineering, Beihang University, Beijing 100083, China*
[2] *No. 61267 Unit of PLA, Beijing, China*

Correspondence should be addressed to Yalin Pan; pyalin@buaa.edu.cn

Received 8 November 2018; Revised 4 March 2019; Accepted 27 March 2019; Published 9 April 2019

Academic Editor: Xesús Nogueira

In this paper, a comprehensive optimization approach is presented to analyze the aerodynamic, acoustic, and stealth characteristics of helicopter rotor blades in hover flight based on the genetic algorithm (GA). The aerodynamic characteristics are simulated by the blade element momentum theory. And the acoustics are computed by the Farassat theory. The stealth performances are calculated through the combination of physical optics (PO) and equivalent currents (MEC). Furthermore, an advanced geometry representation algorithm which applies the class function/shape function transformation (CST) is introduced to generate the airfoil coordinates. This method is utilized to discuss the airfoil shape in terms of server design variables. The aerodynamic, acoustic, and stealth integrated design aims to achieve the minimum radar cross section (RCS) under the constraint of aerodynamic and acoustic requirement through the adjustment of airfoil shape design variables. Two types of rotor are used to illustrate the optimization method. The results obtained in this work show that the proposed technique is effective and acceptable.

1. Introduction

The application of the acoustic and radar stealth technology to helicopter rotors has greatly enhanced the battlefield survivability and the combat effectiveness of helicopters [1]. Research on this technology has always been considered and explored by many different countries. The most effective way to improve the helicopter rotor noise and radar stealth abilities is to reduce their aerodynamic noise and radar scattering characteristics [2–4]. On the one hand, aerodynamic noise is one of the main noise sources of helicopter rotors, including thickness noise, loading noise, and high-speed impulse (HSI) noise. Thickness noise and loading noise belong to the subsonic linear sources, while the helicopter is flying at a low speed [5]. The HSI noise is a particularly intense and annoying noise generated by the helicopter rotor in the high-speed forward flight. The noise is closely associated with the appearance of transonic and supersonic flow around the advancing blades [6]. The prediction of the aerodynamic noise can help or indicate actions or modifications of the designs to reduce the rotor noise. On the other hand, the radar stealth performance is also one of the essential indexes of helicopter rotor design, and acquiring the high-precision response characteristics of RCS is the key in the stealth design of a helicopter rotor [7–9].

In the past few decades, the aerodynamic noise of the helicopter rotor has been calculated by a great number of researchers. A lot of numerical algorithms were proposed based on various solutions of Ffowcs Williams and Hawkings (FW-H) equation [10–12]. Farassat 1, 1a, and Kirchhoff formulation were the most popular. Varieties of methods have also been utilized to compute the RCS of helicopter rotor in the past, such as Physical Optics, Equivalent Currents, Moment, Finite-Difference Time-Domain, and Quasi-Stationary [13–15]. The aerodynamics of helicopter rotor play an essential role in most of the disciplines in helicopter design. There are two common approaches to rotor aerodynamic performance design. One is the experimental method, and the other is the numerical method. The numerical methods, the vortex method and the blade element method, have been commonly utilized in recent years due to their accuracy and convenient implementation [16, 17]. In the modern armed

helicopter rotor design, the aerodynamic, noise, and stealth characteristics should be considered simultaneously. Thereby, the comprehensive analysis about the aerodynamic, noise, and stealth characteristics of helicopter rotor is a challenging multidisciplinary design optimization (MDO) task with great practical value [18].

Currently, the integrated analyses about the aerodynamic and noise optimization, as well as the aerodynamic and stealth optimization of rotor, are discussed in some academic works. In [19], the aerodynamic and acoustic optimization of the rotor blade tip shape is studied with the genetic algorithm based on the Kriging model in detail. The AH-1/OLS rotor is utilized in this study to accomplish the optimization with the aerodynamic performance as a constraint with the minimization of the absolute sound pressure peak value taken as an objective function. Satisfying results are obtained in the optimized simulations. Jiang et al. [20] applied the surrogate model to investigate the integrated optimization analyses of the aerodynamic and stealth characteristics of helicopter rotor. The integration design method proposed by Jiang et al. consists of three modules, including the integrated grids generation, the aerodynamic and stealth solver, and the integrated optimization analysis. By choosing suitable object function and constraint condition, the compromised design about the rotor with high aerodynamic performance and low RCS has been achieved from the numerical simulations. In fact, few papers focus on the comprehensive analysis regarding the aerodynamic, acoustic, and stealth design of the advanced helicopter rotor.

The airfoil shape which significantly affects the aerodynamic, acoustic, and stealth of helicopter rotors is usually considered as a separate problem [21]. In this study, an advanced geometry representation algorithm which utilizes the CST method is adopted to consider the airfoil shape. The superiorities of the CST method are of high accuracy and few design variables are utilized in the geometry representation. To acquire a highly efficient computational method that can be utilized in the MDO design of the rotor, a comprehensive design method based genetic algorithm is proposed to investigate the aerodynamic, acoustic, and stealth of the rotor. First of all, the airfoil shape of the initial rotor is parameterized by utilizing the CST method. On this basis, the aerodynamic characteristics in hover of the rotor are simulated by the blade element momentum theory. The aerodynamic noise of the rotor is calculated by the Farassat 1a formula. The stealth characteristics of the airfoil shape are computed by the method of PO. Then, by choosing the suitable objective function and the constraint condition about the synthesized aerodynamic, noise, and RCS characteristics, the rotor with high aerodynamic performances, low sound pressure level, and low scattering characteristics is designed through the comprehensive analysis.

2. CST Method for Airfoil Shape Parameterization

The CST method was proposed by Kulfan and Bussoletti [23] based on the analytical expressions to represent varieties of shapes with relatively few design variables. The components of the expression are "class function" and "shape function." Each airfoil shape can be defined by the formula

$$\overline{y} = C(\overline{x}) \cdot S(\overline{x}) + \overline{x} \cdot \Delta y_{te} \tag{1}$$

where $C(\overline{x})$ denotes the "class function," $S(\overline{x})$ refers to the "shape function" $\overline{x} \in [0, 1]$, and Δy_{te} is the trailing-edge thickness.

For the upper and lower surface of the airfoil, one has

$$\overline{y}_u = C(\overline{x}) \cdot S(\overline{x}) + \overline{x} \cdot \Delta y_{te,u} \tag{2}$$

$$\overline{y}_l = C(\overline{x}) \cdot S(\overline{x}) + \overline{x} \cdot \Delta y_{te,l} \tag{3}$$

where $\overline{y}_u$ is the curve coordinates of the upper surface of airfoil, $\overline{y}_l$ means the curve coordinates of lower surface of airfoil, $\Delta y_{te,u}$ refers to the trailing-edge half-thickness of upper surface of airfoil, and $\Delta y_{te,l}$ means the trailing-edge half-thickness of lower surface of airfoil.

The "class function" is shown by the formula

$$C(\overline{x}) = (\overline{x})^{N_1} \cdot (1 - \overline{x})^{N_2}, \quad 0 \le \overline{x} \le 1 \tag{4}$$

The values of N_1 and N_2 control the overall shape of the parameterization, and $N_1 = 0.5$, $N_2 = 1$ in this paper.

The "shape function" can be given by the linear combination of Bernstein polynomials, that is,

$$S(\overline{x}) = \sum_{i=0}^{N_b} A_i \cdot B_i(\overline{x}) \tag{5}$$

in which

$$B_i(\overline{x}) = \binom{N_b}{i} \overline{x}^i (1 - \overline{x})^{n-i} \tag{6}$$

A_i is the Bernstein coefficient, and N_b refers to the degree of polynomials. Using (2) and (3), any airfoil shape can be parameterized easily.

Substituting the point $\overline{x}_i \in [0, 1]$ into (2) and (3), one can obtain $2N_b + 2$ unknown coefficients A_i and $\Delta y_{te,u}$, $\Delta y_{te,l}$ by solving a system of algebraic equations. These coefficients are also the design variables of the airfoil. The "NACA 0012" and "ONERA OA213" airfoils are selected to verify the correctness of the CST method. Figures 1 and 2 present the airfoil geometry with the usage of the CST method.

3. Numerical Methods

3.1. Blade Element Momentum Theory. The blade element momentum theory is a combination of the momentum theory and the blade element theory. In this method, the rotor blades are divided into a number of independent elements along the length of blade. For each section, the momentum theory is the control volume theory, and the blade element theory is the summation of the sectional thrust and torque as computed by the sectional lift and drag coefficient of the airfoil.

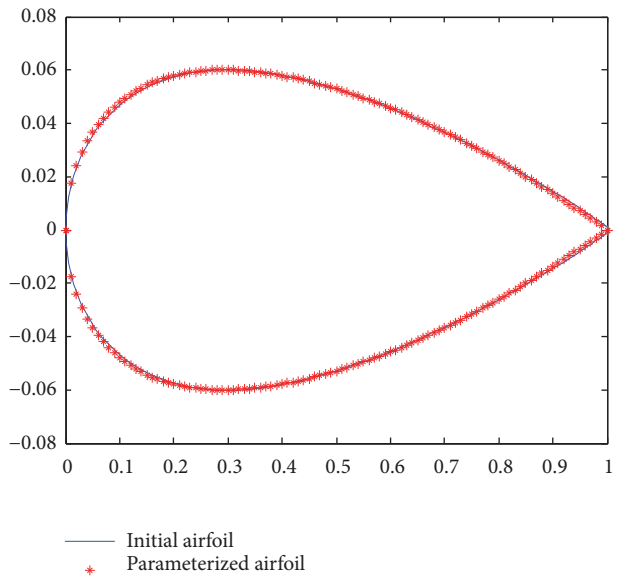

Figure 1: NACA 0012 airfoil representation.

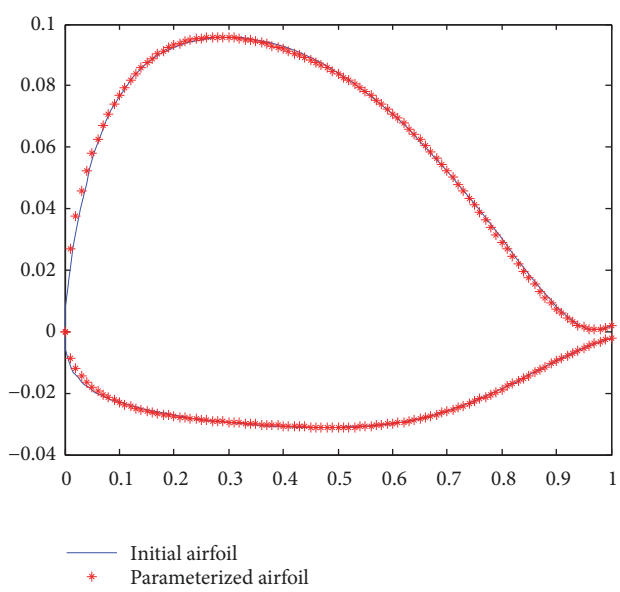

Figure 2: ONERA OA213 airfoil representation.

The thrust and the torque according to the momentum theory are as follows:

$$dT = 2\rho\left(2\pi r \cdot dr\right)\left(V_0 + v_1\right)v_1 \tag{7}$$

$$dM = 4\pi\rho r^3 v_1 b\Omega \cdot dr \tag{8}$$

where dT is the element thrust, ρ denotes the fluid density, v_1 refers to the induced velocity at the disc, V_0 means the reference upstream velocity, $V_0 = 0$ is in the hover flight, r is the local element mean radius, dr is the radial length of each ring, dM denotes the element torque, b means the tangential induction factor that expresses the change in tangential velocity, and Ω is the angular velocity of the rotor [24].

By the blade element theory, the aerodynamic lift and drag forces on the airfoil are expressed by the formula as follows:

$$dY = \frac{1}{2}C_l\rho W^2 c dr \tag{9}$$

$$dX = \frac{1}{2}C_d\rho W^2 c dr \tag{10}$$

where W is the resultant fluid velocity, c is the blade chord, and the coefficients of lift (C_l) and drag (C_d) are input from two-dimensional airfoil data from the Xfoil software. Then the thrust and the torque according to the blade element theory are obtained as follows [25]:

$$dT_k = \frac{1}{2}\rho W^2 kc\left(C_l\cos\phi + C_d\sin\phi\right)dr \tag{11}$$

$$dM_k = \frac{1}{2}\rho W^2 kc\left(C_l\sin\phi - C_d\cos\phi\right)rdr \tag{12}$$

where k is the number of the blades and $\phi = \arctan((V_0 + v_1)/r\Omega)$ denotes the inflow angle. Figure 3 shows the description of the airfoil.

Integrating (11) and (12) with the total blade, the total thrust and total torque are given by

$$T = \int dT_k \tag{13}$$

$$M = \int dM_k \tag{14}$$

The thrust coefficient is

$$C_T = \frac{T}{(1/2)\rho\pi R^2(\Omega R)^2} \tag{15}$$

in which R denotes the radius of the disc.

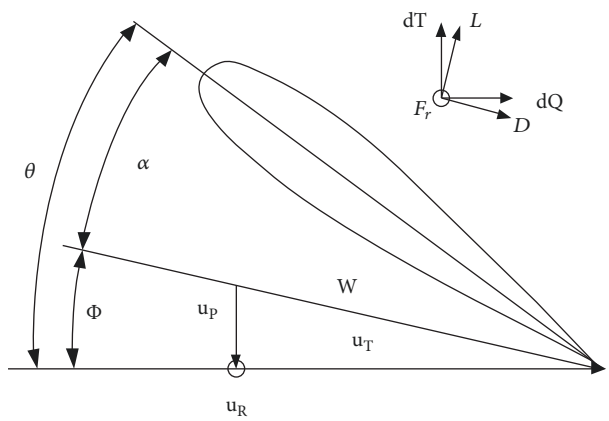

Figure 3: Blade element profile.

To solve the total thrust or the thrust coefficient, the induced velocity v_1 should be obtained first. Putting (7) and (11) together, the induced velocity can be obtained with the usage of the Newton iteration method.

3.2. Farassat Theory. Aeroacoustic analogy can be utilized to investigate the problem of aerodynamic noise, and the FW-H equation is adopted to calculate the free-field acoustic noise. The FW-H equation is a reorganization of the Navier-Stokes equations. The derivation of the FW-H equation uses generalized function theory which is an elegant element of mathematics. The most important characteristic of the FW-H equation is that it can address acoustic propagation generated from a moving surface. Since the influence of quadrupole source is negligible for the low rotary speed blade, the simplification form of the FW-H equation is given as follows [12]:

$$\left(\frac{1}{c_0^2}\frac{\partial^2}{\partial t^2}-\frac{\partial^2}{\partial x_i^2}\right)p'(x,t) = \frac{\partial}{\partial t}\left[\rho_0 U_n \delta(f)\right]-\frac{\partial}{\partial x_i}\left[L_i\delta(f)\right] \tag{16}$$

with

$$U_n = U_i\hat{n}_i,\qquad U_i = \left[1-\left(\frac{\rho}{\rho_0}\right)\right]v_i+\left(\frac{\rho u_i}{\rho_0}\right) \tag{17}$$

Equation (16) can be solved by the famous Farassat 1 and Farassat 1a formulation in time domain [26]. Equation (16) can be solved by utilizing the formulation of Farassat 1a, which is given as follows:

$$p'(x,t) = p_T'(x,t)+p_L'(x,t) \tag{18}$$

with

$$\begin{aligned}4\pi p_T'(x,t) &= \int_S\left[\frac{\rho_0\left(\dot{U}_n+U_{\dot{n}}\right)}{r\left(1-M_r\right)^2}\right]_{ret}dS \\ &\quad+\int_S\left[\frac{\rho_0 U_n\left(r_i\dot{M}_i+c_0M_r+c_0M^2\right)}{r^2\left(1-M_r\right)^3}\right]_{ret}dS\end{aligned} \tag{19}$$

$$\begin{aligned}4\pi p_L'(x,t) &= \frac{1}{c_0}\int_S\left[\frac{\dot{L}_r}{r\left(1-M_r\right)^2}\right]_{ret}dS \\ &\quad+\int_S\left[\frac{L_r-L_M}{r^2\left(1-M_r\right)^2}\right]_{ret}dS \\ &\quad+\frac{1}{c_0}\int_S\left[\frac{L_r\left(r\dot{M}_r+c_0M_r-c_0M^2\right)}{r^2\left(1-M_r\right)^3}\right]_{ret}dS\end{aligned} \tag{20}$$

where $p_T'(x,t)$ represents the thickness sound pressure, $p_L'(x,t)$ denotes the loading sound pressure, ρ_0 and c_0 are the fluid and sound speed, respectively, L represents the aerodynamic pressure with $L_i = P_{ij}\hat{n}_j + \rho u_i(u_n - v_n)$, u_i is the fluid velocity, and v_i stands for the velocity of the surface. The relative speed $(u_i - v_i)$=0 and U_i are reduced to $U_i = v_i$ when the control surface is solid. M represents the local Mach number vector of source with respect to a frame fixed to the undisturbed medium with components M_i. And the subscript r denotes projection onto the source observer direction. The subscript M represents the projection on the Mach number vector. For a low speed rotor application in this paper, monopole source is the dominant and dipole source while quadrupole source is shown to be negligible. Thereby, the thickness noise of the rotor would be taken into consideration only.

3.3. RCS Method. The total RCS of the rotor could be computed as the sum of surfaces and edges. The scattering field of the surfaces and edges is calculated by PO and MEC, respectively. The initial point of PO is the surface currents produced by an incoming electromagnetic wave. To improve the PO solution and take into account the diffraction by edges, the MEC has been proposed by Michaeli [27]. The MEC describes the source of the field in terms of fictitious equivalent electric and magnetic currents along the edge. Some necessary mathematical preliminaries of the PO and MEC theory are given in the following sections [28, 29].

3.3.1. Physical Optics Method. Stratton and Chu [30] derived an exact solution to the scattered field by applying the vectorial analog of the Green theorem to the Maxwell equations. These integral equations, as follows, do not usually have an analytical solution.

$$\boldsymbol{E}^s = \oint_S\left[j\omega\mu(\boldsymbol{n}\times\boldsymbol{H})+(\boldsymbol{n}\times\boldsymbol{E})\times\nabla\psi+(\boldsymbol{n}\cdot\boldsymbol{E})\nabla\psi\right]dS \tag{21}$$

$$\boldsymbol{H}^s = \oint_S\left[j\omega\xi(\boldsymbol{n}\times\boldsymbol{E})+(\boldsymbol{n}\times\boldsymbol{H})\times\nabla\psi+(\boldsymbol{n}\cdot\boldsymbol{H})\nabla\psi\right]dS \tag{22}$$

where $\psi = e^{jkR}/4\pi R$ is Green's function of free space, $\boldsymbol{E}^s$ and $\boldsymbol{H}^s$ are the scattered electric and magnetic field, respectively,

Table 1: The main parameters of the rotor.

Total weight	Rotor shape	Number of blades	Radius of blades	Chord length of blades
9071.8kg	Rectangle	4	9.144m	0.6096m
Rotor solidity	Root cut ratio	Negative twist	Tip speed	Airfoil shape
0.085	0.15	-10°	198.12m/s	NACA 0012

Table 2: The comparison of the calculated results and the results in [22].

	Results in Ref.[22]	Calculated results
Thrust coefficient	0.01438	0.01485
Torque coefficient	0.00119	0.00122
Hover efficiency	72.45%	74.78%

$\boldsymbol{E}$ and $\boldsymbol{H}$ stand for the total electric and magnetic fields, respectively, μ and ξ are relative permeability and permittivity, respectively, $\boldsymbol{n}$ denotes an outward surface normal erected on the surface element dS, and ω refers to the angular frequency.

3.3.2. Method of Equivalent Currents. In this paper, simple diffractions by edges are treated with the usage of the formulation of equivalent currents proposed by Mitzner [27]. The scattered field of the equivalent line can be written as

$$\boldsymbol{E}_d = -jk\psi_0 \int_l \left[Z_0 I^e \boldsymbol{s}\times(\boldsymbol{s}\times\boldsymbol{t}) + I^m \boldsymbol{s}\times\boldsymbol{t}\right] \frac{1}{\sin\theta} e^{-jk\boldsymbol{r}\cdot\boldsymbol{s}} dz \tag{23}$$

where I^e and I^m are equivalent line electrical and magnetic currents, respectively, Z_0 denotes the impedance of free space, $k = 2\pi/\lambda$ and λ are the wavelength, dz denotes the length of ledge, $\boldsymbol{t}$ represents the unit vector along edge direction, $\boldsymbol{s}$ is the unit vector along diffraction direction, and $\boldsymbol{r}$ means the position vector of reference point of target.

Solving (21), (22), and (23) numerically, the RCS of the rotor can be obtained. And the solving process can be found in [30].

After the RCS of n face elements and m edges of the rotor are calculated, the total RCS of the target can be acquired as follows:

$$\sigma = \left|\sum_{i=1}^{n}\left(\sqrt{\sigma_f}\right)_i + \sum_{j=1}^{m}\left(\sqrt{\sigma_s}\right)_j\right|^2 \tag{24}$$

where σ_f is the RCS of rotor surface obtained by PO and σ_s denotes the RCS of rotor edges obtained by MEC.

4. Results and Discussions

4.1. Test Case. In the aerodynamic case, the rotor of [22] is selected to verify the effectiveness of the blade element momentum theory in hover. The parameters of the rotor are displayed in Table 1.

Table 2 shows the calculated aerodynamic characteristics, including the thrust coefficient, the torque coefficient, and the hover efficiency. From Table 2, one can find that the calculated results are in good agreement with the results in [22]. It has been demonstrated that the approach is suitable for solving the aerodynamic characteristics of rotor.

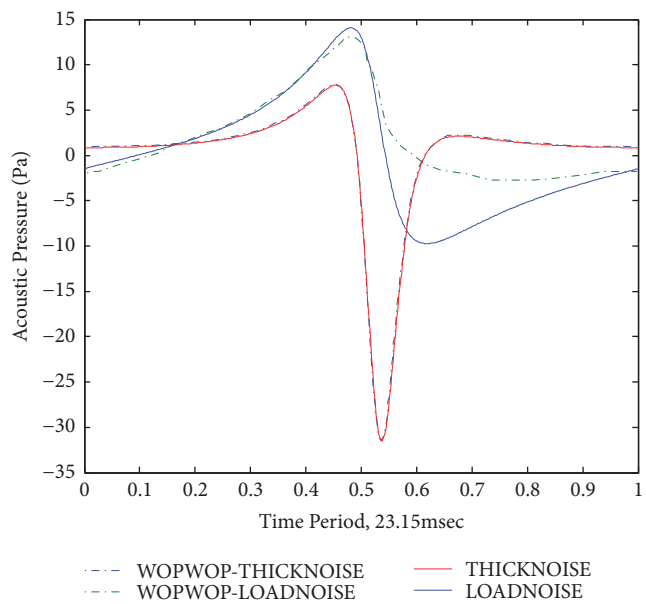

Figure 4: The comparison of the calculated results and WOPWOP code results.

In the aerodynamic noise case, the Farassat 1a is utilized to compute the thickness noise and the loading noise of the Caradonna-Tung rotor (C-T rotor) (parameters of the C-T rotor are shown in Table 3), and to compare the results with the widely used WOPWOP code [31], which is a computational aeroacoustics code based on the Farassat 1a. Figure 4 presents the calculated results and the WOPWOP code results.

It can be seen that the thickness noise is in good coincidence with the WOPWOP code results. There are discrepancies between the calculated loading noise and the WOPWOP code results because of different methods to calculate the rotor's aerodynamic characteristics. Since the sound pressure level of thickness noise is much bigger than the loading noise, thickness noise is only considered as the acoustic constraints.

Table 3: The main parameters of C-T rotor.

Rotor shape	Number of blades	Radius of blades	Chord length of blades
Rectangle	2	1.143m	0.1905m
Aspect ratio	Pitch angle	Rotation speed	Airfoil shape
6	8°	1250rpm	NACA 0012

Table 4: The main parameters of the 5-rotor.

Rotor shape	Number of blades	Radius of blades	Chord length of blades
Rectangle	5	6.595m	0.4m
Pitch angle	Rotation speed	Rotation period	Airfoil shape
12°	1250rpm	0.048s	ONERA OA213

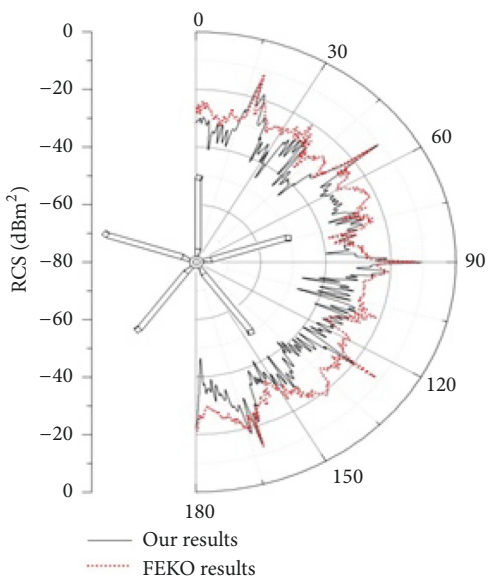

Figure 5: The comparison of the calculated results and the FEKO results at f=3 GHz.

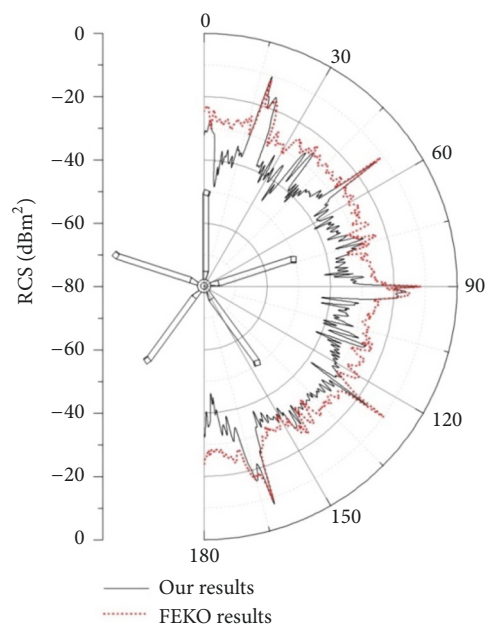

Figure 6: The comparison of the calculated results and the FEKO results at f=6 GHz.

In the RCS case, a 5-rotor is selected to illustrate the validity of the PO and MEC under the conditions of radar frequency of f=3 GHz and f=6GHz with vertical polarization, respectively. The main parameters of the rotor are displayed in Table 4. Figures 5 and 6 present the comparison between the calculated results and FEKO results (FEKO: A commercial software, Fast multipole method is used [32]) for different frequencies. The peak of the RCS for varieties of methods is very consistent, and the tendency of the RCS is similar to each other by taking a closer look at Figures 5 and 6. The averages of the RCS from 0° to 180° between ours and FEKO results are both less than 1.5dB, which are accepted in engineering.

4.2. Comprehensive Design of Aerodynamic, Acoustic, and Stealth of Rotor. The comprehensive analysis about the aerodynamic, acoustic, and stealth characteristics of the rotor is an MDO issue, and the blade shapes of rotor to improve the aerodynamic performance and reduce the noise and RCS at the same time are generally inconsistent. Therefore, the key is to search the aerodynamic, acoustic, and stealth compromised results which can be described as the optimal solution. For this MDO issue, the mathematical model should be established first. Due to the influence of airfoil shape on aerodynamic, thickness noise, and scattering characteristics of rotor, the optimized rotor can be designed by the means of optimizing the airfoil shape. Subsequently, the objective function is as follows:

$$\max -10\log_{10}\left(Average\left(RCS\left(\overrightarrow{X}\right)\right)\right) \tag{25}$$

where $RCS(\overrightarrow{X})$ denotes the RCS of airfoil, and the design variables are

$$\overrightarrow{X} = \{\overline{x}_i\}, \quad i = 1, 2, 3, \ldots 2N_b + 4 \tag{26}$$

where x_i is the coefficient of the airfoil parameterization, and the constraint condition is

Table 5: The range of the design variables of C-T rotor.

Variables	$\overline{x}_1$	$\overline{x}_2$	$\overline{x}_3$	$\overline{x}_4$	$\overline{x}_5$	$\overline{x}_6$	$\overline{x}_7$	$\overline{x}_8$
Lower bound	0.1	0.1	0.1	0.1	-0.1	-0.1	-0.1	-0.1
Upper bound	0.2	0.2	0.2	0.2	-0.2	-0.2	-0.2	-0.2

Table 6: The comparison of the initial design variables and the optimized design variables for C-T rotor.

Variables	$\overline{x}_1$	$\overline{x}_2$	$\overline{x}_3$	$\overline{x}_4$	$\overline{x}_5$	$\overline{x}_6$	$\overline{x}_7$	$\overline{x}_8$
Initial	0.177	0.1458	0.1462	0.1445	-0.177	-0.1458	-0.1462	-0.1445
Optimized	0.1173	0.1563	0.1224	0.1956	-0.116	-0.1022	-0.1886	-0.1633

Table 7: The comparisons of the aerodynamic characteristic and the noise between initial and optimized for C-T rotor.

	Thrust /N	Thrust coefficient	SPL/dB
Initial	1099.7	0.0614	96.50
Optimized	1256.3	0.0701	95.08

$$\begin{aligned} C_T &\geq C_{T0} \\ SPL_H &< SPL_{H0} \\ x_{iL} &\leq \overline{x}_i \leq x_{iU} \end{aligned} \tag{27}$$

where C_T and C_{T0} denote the post-optimization and initial rotor thrust coefficient in hover, respectively. SPL_H and SPL_{H0} denote the post-optimization and initial rotor thickness noise, respectively. x_{iL} and x_{iU} denote the lower bound and upper bound of each design variable, individually. The thrust coefficient is calculated by the blade element momentum theory, the thickness noise is computed by Farassat 1a, and the stealth characteristic is approximated by PO. GA, as global optimization method, uses the objective function and searchers from the population of points [33]. It is a search algorithm based on the principles of natural selection and natural genetics. GA uses three elements: reproduction, crossover, and mutation. Reproduction is a process in which individual chromosomes in a population are copied according to their objective function values [34]. Crossover is the exchange of genes between the parent chromosomes. Mutation refers to a genetic change in a chromosome to prevent GA from failing into the local optima [35]. In this section, binary code is used, the population crossover probability is 0.8, mutation probability is 0.01, the population size is 100, and the genetic number is 200. The flowchart of the comprehensive analysis of aerodynamic, acoustic, and stealth of rotor based on GA is given in Figure 7. Next, the test case of the C-T rotor and 5-rotor is utilized to optimize design, respectively.

4.2.1. C-T Rotor Case. According to Table 3, the airfoil of the C-T rotor is NACA 0012, take $N_b = 3$, parameterizing this airfoil by CST. Since the thickness of the trailing-edge of NACA 0012 is equal to zero, $\Delta y_{te,u} = 0$ and $\Delta y_{te,l} = 0$. Thereby, 8 design variables are needed to parameterize NACA 0012. Table 5 presents the range of these design variables.

Using the blade element momentum theory, the initial C-T rotor thrust coefficient is 0.0614. The initial C-T rotor thickness noise is 96.50dB at the 1th blade pass frequency (BPF) by Farassat 1a. Figure 8 presents the comparison of the initial airfoil and the optimized airfoil. The comparisons of design variables between the initial airfoil and optimized airfoil are established in Table 6.

Figure 9 indicates the comparisons of the RCS characteristics (f=10GHz with vertical polarization) between the initial and optimized airfoil. When compared with the stealth characteristics of initial rotor, the RCS reduction effect of the optimized airfoil is very obvious at the trough, and it nearly decreases by 5dBsm (maximum). According to Figure 9, the omnidirectional mean of airfoil RCS before optimizing is -19.37dBsm, and the omnidirectional mean of airfoil RCS after optimizing is -21.05dBsm, decreased by 1.68dBsm.

The RCS of the C-T rotor at f=10GHz with vertical polarization for initial and optimized airfoil is shown in Figure 10. From Figure 10, one can find that the RCS reduction effect of C-T rotor is outstanding in the majority azimuths. The omnidirectional mean of C-T rotor RCS before optimizing is -19.33dBsm, and the omnidirectional mean of airfoil RCS after optimizing is -22.42dBsm, decreased by 3.09dBsm. As a result, it is demonstrated that the optimal method can satisfy the RCS reduction requirements in the practical applications.

The aerodynamic characteristic and the noise of the C-T rotor are displayed in Table 7. When compared with the aerodynamic characteristics of the initial C-T rotor, the thrust and thrust coefficient increase. However, the sound pressure level (SPL) of the thickness noise is reduced by 1.42dB. Figures 11 and 12 present the comparison of the SPL's curve for the time-frequency domain. It can be concluded that the noise of the optimized C-T rotor decreases at many points. It is further illustrated that the optimal method can obtain better aerodynamic characteristics as well as the lower noise and RCS.

4.2.2. 5-Rotor Case. Since the airfoil of the 5-rotor is ONERA OA213 (see Table 4), the shape of this airfoil is rather complex, and $\Delta y_{te,u} \neq 0$, $\Delta y_{te,l} \neq 0$. Thus, in $N_b = 4$, there are 12 design variables for parameterizing this airfoil by the means of CST. The range of each design variable is displayed in Table 8.

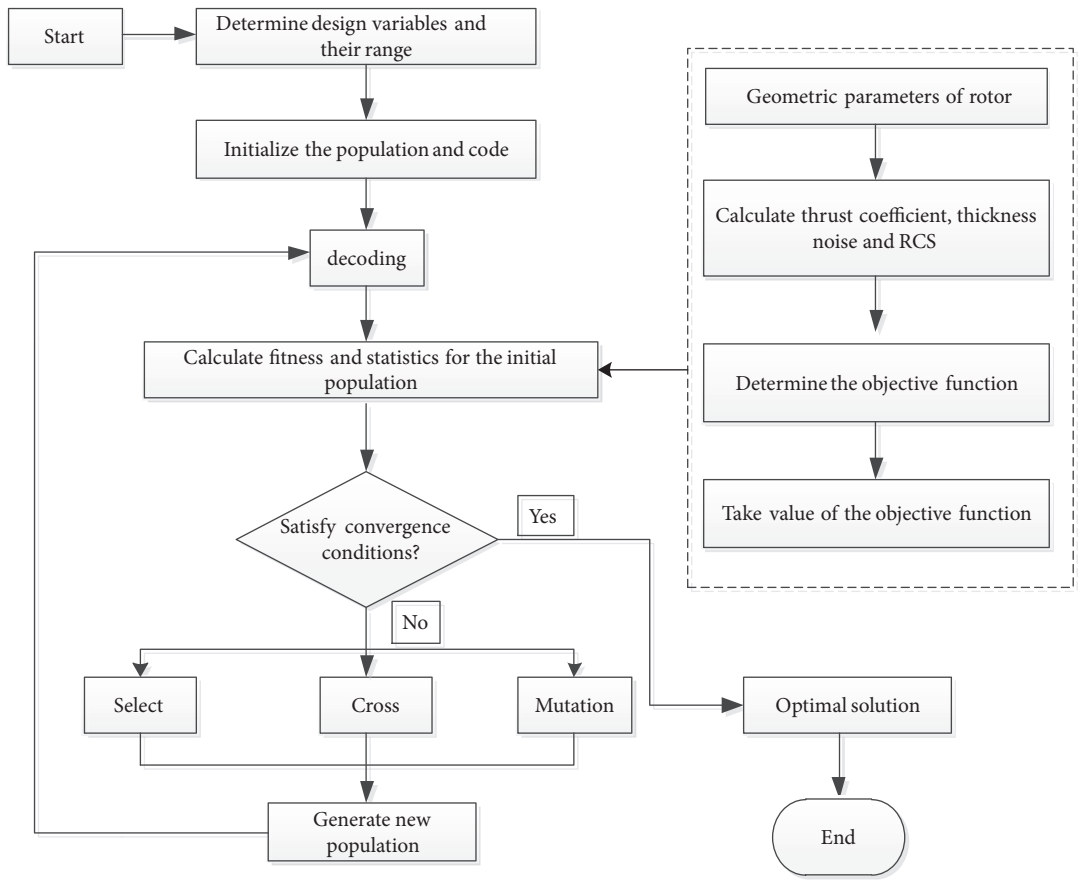

Figure 7: The flowchart of the comprehensive analysis of the aerodynamic, acoustic, and stealth of rotor based on GA.

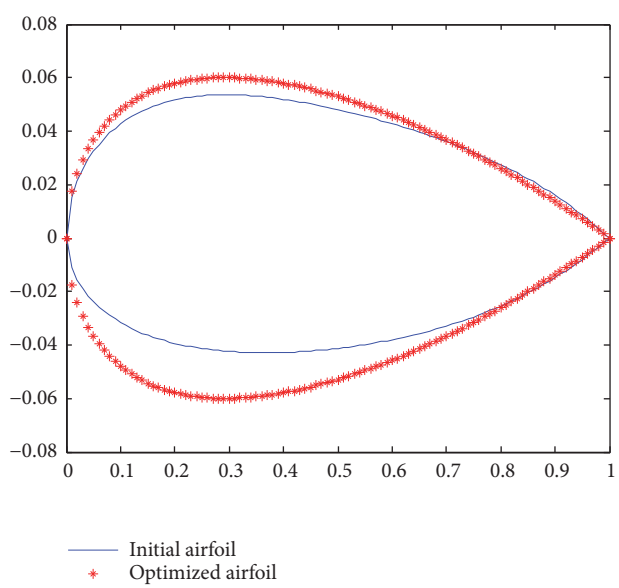

Figure 8: The comparison of airfoil between initial airfoil and optimized airfoil for C-T rotor.

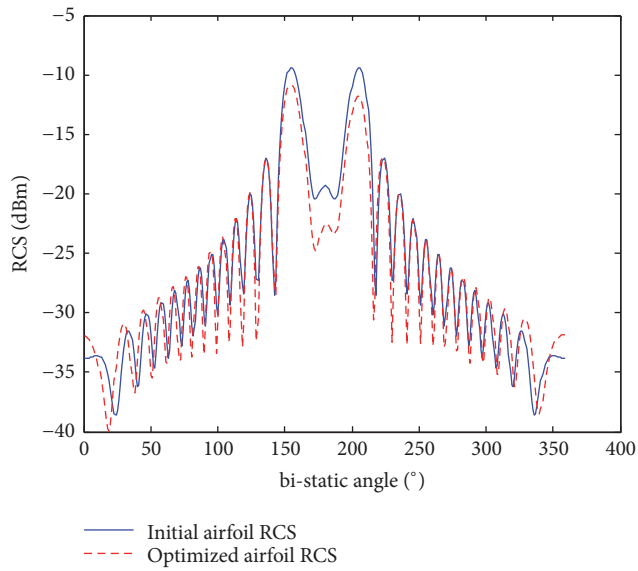

Figure 9: The comparisons of RCS characteristics between the initial and optimized airfoil for C-T rotor.

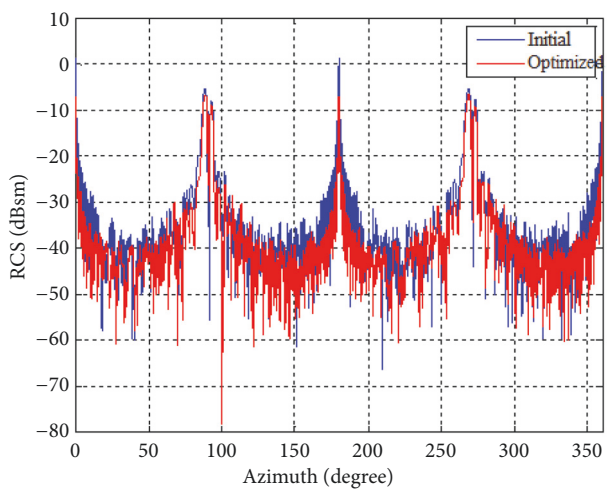

Figure 10: The comparisons of the RCS characteristics between the initial and optimized C-T rotor.

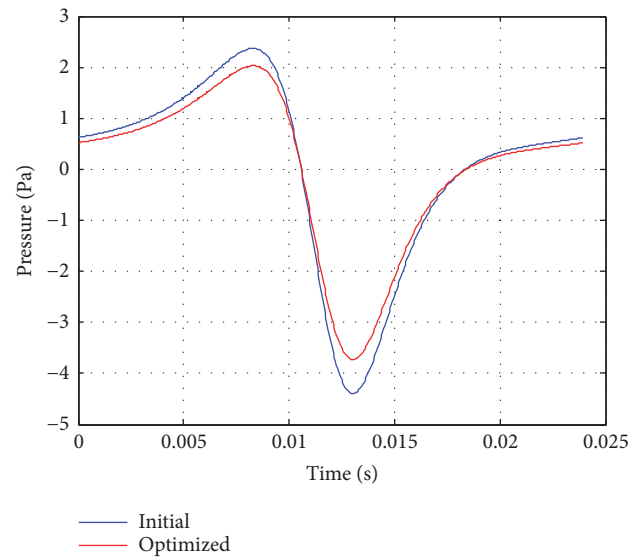

Figure 11: The comparisons of the thickness noise between the initial and optimized C-T rotor for time domain.

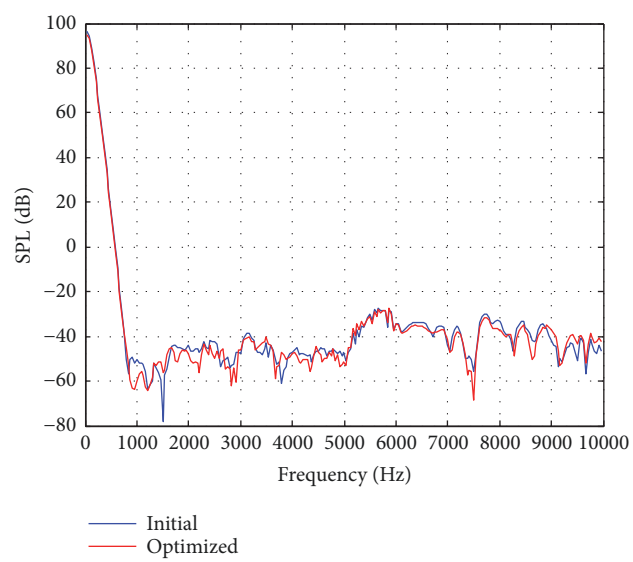

Figure 12: The comparisons of the thickness noise between the initial and optimized C-T rotor for frequency domain.

Utilizing the same method to optimize this airfoil, one can compare the initial airfoil and the optimized airfoil, which is given by Figure 13.

The comparisons of the design variables between the initial airfoil and the optimized airfoil are displayed in Table 9.

Figure 14 displays the comparisons of RCS (f=10GHz with vertical polarization) between the initial and optimized airfoil. Compared with the RCS characteristics of initial rotor, the RCS reduction effect of the optimized airfoil is very obvious at the lower surface of airfoil. In Figure 14, the omnidirectional mean of airfoil RCS before optimizing is -17.35dBsm, and the omnidirectional mean of airfoil RCS after optimizing is -18.29dBsm, decreased by 0.94dBsm.

The RCS of the 5-rotor at f=10GHz with vertical polarization for the initial and optimized airfoil is displayed in Figure 15. From Figure 15, one can see that the RCS reduction effect of 5-rotor is remarkable at the peak and trough. The omnidirectional mean of 5-rotor RCS before optimizing is -5.9dBsm, and the omnidirectional mean of the airfoil RCS after optimizing is -7.31dBsm, decreased by 1.41dBsm.

The aerodynamic characteristic and the noise of 5-rotor are presented in Table 10. When compared with the aerodynamic characteristics of the initial C-T rotor, the thrust and thrust coefficient also become large, and the SPL of the thickness noise is reduced by 0.36dB slightly. Figures 16 and 17 display the comparisons of the SPL's curve for the time-frequency domain. The same conclusion in Section 4.2.1 would be acquired again.

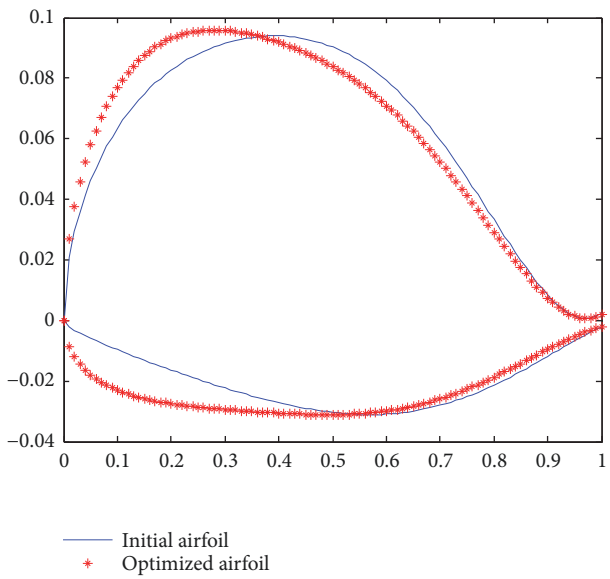

Figure 13: The comparison of airfoil between initial airfoil and optimized airfoil for 5-rotor.

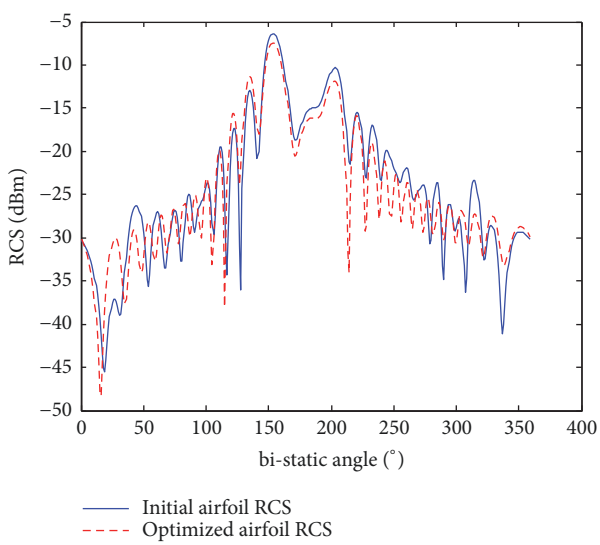

Figure 14: The comparisons of the RCS characteristics between the initial and optimized airfoil for C-T rotor.

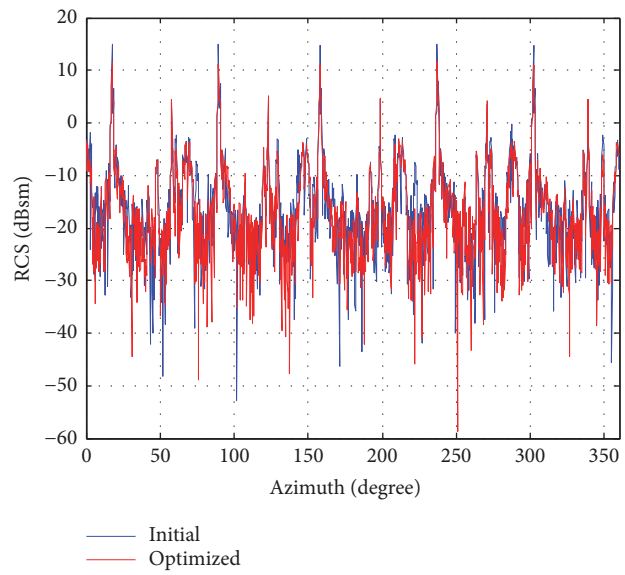

Figure 15: The comparisons of the RCS characteristics between the initial and optimized 5-rotor.

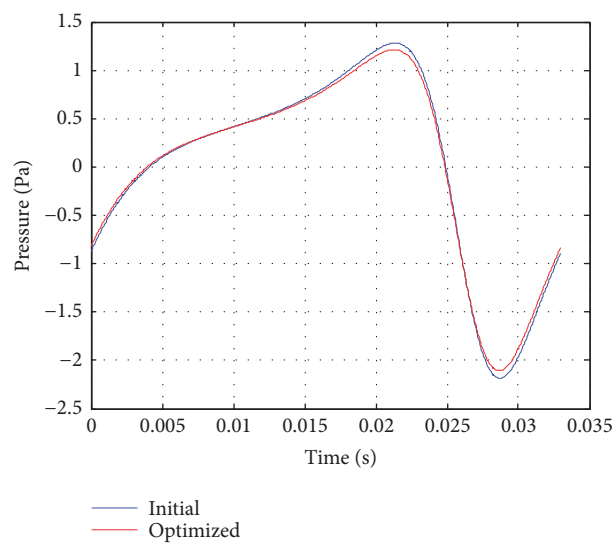

Figure 16: The comparisons of the thickness noise between the initial and optimized 5-rotor for time domain.

Generally, results indicate that the airfoil shape design of rotor with high aerodynamic performances, low noise, and low scattering characteristics has been given, which shows that the optimization strategy in this article is feasible and credible.

5. Conclusion

An automated process for the comprehensive optimization design of the aerodynamic, acoustic, and stealth characteristics of the rotor is developed in the article. The airfoil curve is represented by utilizing the CST method with few design variables, which is reasonable for the performance of the optimization problem. The aerodynamic, acoustic, and stealth characteristics of the rotor in hover are simulated effectively by utilizing the blade element momentum theory, Farassat 1a, PO, and MEC, respectively. Optimizing the design variables of airfoil by objective function with constraints, based on GA, a new airfoil could be acquired. Adopting the new airfoil to the rotor, another new rotor with high aerodynamic characteristics, low noise, and low RCS would be achieved. The proposed comprehensive optimization design method is suitable for the preliminary design phase where there is a need for quick estimation in consideration of the aerodynamic, acoustic, and stealth factors.

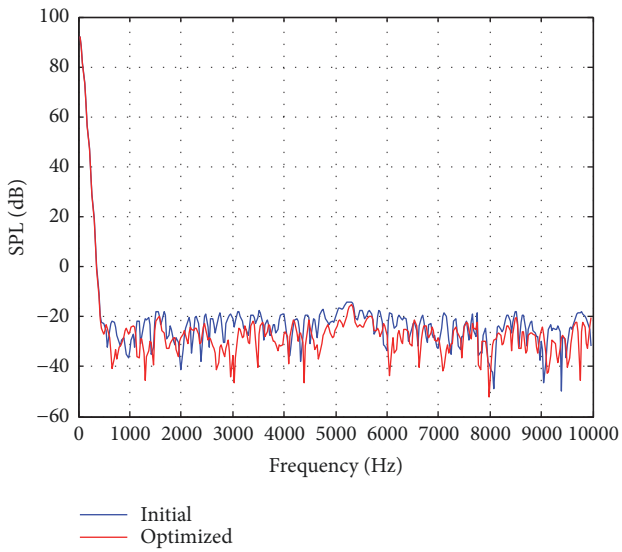

Figure 17: The comparisons of the thickness noise between the initial and optimized 5-rotor for frequency domain.

Table 8: The range of the design variables of 5-rotor.

Variables	Lower bound	Upper bound
$\overline{x}_1$	0.2	0.3
$\overline{x}_2$	0.2	0.3
$\overline{x}_3$	0.1	0.2
$\overline{x}_4$	0.4	0.5
$\overline{x}_5$	-0.1	-0.2
$\overline{x}_6$	-0.01	-0.15
$\overline{x}_7$	-0.01	-0.1
$\overline{x}_8$	-0.01	-0.1
$\overline{x}_9$	-0.1	-0.2
$\overline{x}_{10}$	-0.01	-0.1
$\overline{x}_{11}$	0.002	0.003
$\overline{x}_{12}$	-0.002	-0.003

Table 9: The comparison of the initial design variables and optimized design variables for 5-rotor.

Variables	Initial	Optimized
$\overline{x}_1$	0.2708	0.2079
$\overline{x}_2$	0.2876	0.2598
$\overline{x}_3$	0.1293	0.1718
$\overline{x}_4$	0.4124	0.4688
$\overline{x}_5$	-0.1048	-0.1220
$\overline{x}_6$	-0.0881	-0.0202
$\overline{x}_7$	-0.0668	-0.0565
$\overline{x}_8$	-0.0524	-0.0586
$\overline{x}_9$	-0.1609	-0.1604
$\overline{x}_{10}$	-0.0475	-0.0816
$\overline{x}_{11}$	0.0021	0.0023
$\overline{x}_{12}$	-0.0021	-0.0022

Table 10: The comparisons of the aerodynamic characteristic and the noise between the initial and optimized 5-rotor.

	Thrust /N	Thrust coefficient	SPL/dB
Initial	40424	0.0364	92.35
Optimized	42448	0.0382	91.99

Data Availability

The data used to support the findings of this study are available from the corresponding author upon request.

Conflicts of Interest

The authors declare that they have no conflicts of interest.

References

[1] W. Johnson, *Helicopter Theory*, Princeton University Press, 1980.

[2] M. S. Murugan, R. Ganguli, and D. Harursampath, "Surrogate based design optimisation of composite aerofoil cross-section for helicopter vibration reduction," *The Aeronautical Journal*, vol. 116, no. 1181, pp. 709–725, 2012.

[3] A. Le Pape and P. Beaumier, "Numerical optimization of helicopter rotor aerodynamic performance in hover," *Aerospace Science and Technology*, vol. 9, no. 3, pp. 191–201, 2005.

[4] K. S. Brentner and F. Farassat, "Helicopter noise prediction: The current status and future direction," *Journal of Sound and Vibration*, vol. 170, no. 1, pp. 79–96, 1994.

[5] K. S. Brentner, G. A. Brès, G. Perez et al., "Maneuvering rotorcraft noise prediction: a new code for a new problem," in *Proceedings of the AHS Aerodynamics, Acoustics, and Test Evaluation Specialist Meeting*, 2002.

[6] K. S. Brentner, "An efficient and robust method for predicting helicopter high-speed impulsive noise," *Journal of Sound and Vibration*, vol. 203, no. 1, pp. 87–100, 1997.

[7] M. Yi, J. Huang, and Z. Meng, "A cancelling method based on Nth-order SSC algorithm for solving active cancellation problems," *Aerospace Science and Technology*, vol. 71, pp. 264–271, 2017.

[8] P. Pouliguen, L. Lucas, F. Muller, S. Quete, and C. Terret, "Calculation and analysis of electromagnetic scattering by helicopter rotating blades," *IEEE Transactions on Antennas and Propagation*, vol. 50, no. 10, pp. 1396–1408, 2002.

[9] V. Chen, F. Li, S. Ho, and H. Wechsler, "Analysis of micro-Doppler signatures," *IEE Proceedings—Radar, Sonar and Navigation*, vol. 150, no. 4, pp. 271–276, 2003.

[10] J. E. Ffowcs Williams and D. L. Hawking, "Sound generated by turbulence and surfaces in arbitrary motion," *Philosophical Transactions of the Royal Society A: Mathematical, Physical & Engineering Sciences*, vol. A264, no. 1511, pp. 321–342, 1969.

[11] F. Farassat, "Linear acoustic formulas for calculation of rotating blade noise," *AIAA Journal*, vol. 19, no. 9, pp. 1122–1130, 1981.

[12] F. Farassat and M. K. Myers, "Extension of Kirchhoff's formula to radiation from moving surfaces," *Journal of Sound and Vibration*, vol. 123, no. 3, pp. 451–460, 1988.

[13] Y. Shaobo and X. Junjiang, "Geometric optimization design system incorporating hybrid GRECO-WM scheme and genetic algorithm," *Chinese Journal of Aeronautics*, vol. 22, no. 6, pp. 599–606, 2009.

[14] S. B. Ye and J. J. Xiong, "Dynamic RCS behavior of helicopter rotating blades," *Journal of Aeronautics*, vol. 27, no. 5, pp. 816–822, 2006.

[15] X. Bao, Y. Zhang, and X. Du, "Radar scattering characteristics and RCS reduction of utility helicopter," *Journal of Beijing University of Aeronautics and Astronautics*, vol. 39, no. 6, pp. 745–750, 2013.

[16] A. T. Conlisk, "Modern helicopter rotor aerodynamics," *Progress in Aerospace Sciences*, vol. 37, no. 5, pp. 419–476, 2001.

[17] P. Joncheray, "Aerodynamics of helicopter rotor in hover: The lifting-vortex line method applied to dihedral tip blades," *Aerospace Science and Technology*, vol. 1, no. 1, pp. 17–25, 1997.

[18] O. De Weck, J. Agte, J. Sobieszczanski-Sobieski, P. Arendsen, A. Morris, and M. Spieck, "State-of-the-art and future trends in multidisciplinary design optimization-review," in *Proceedings of the 48th AIAA/ASME/ASCE/AHS/ASC Structures, Structural Dynamics, and Materials Conference*, Honolulu, HI, USA, 2007.

[19] W. L. Guo, W. P. Song et al., "An effective aerodynamics/Acoustic optimization of blade tip planform for helicopter rotors," *Journal of Northwestern Polytechnical Univeristy*, vol. 30, no. 1, pp. 73–79, 2012.

[20] X. Jiang, Q. Zhao, G. Zhao, and P. Li, "Integrated optimization analyses of aerodynamic/stealth characteristics of helicopter rotor based on surrogate model," *Chinese Journal of Aeronautics*, vol. 28, no. 3, pp. 737–748, 2015.

[21] N. A. Vu and J. W. Lee, "Aerodynamic design optimization of helicopter rotor blades including airfoil shape for forward flight," *Aerospace Science and Technology*, vol. 42, pp. 106–117, 2015.

[22] Z. Gao et al., *The Helicopter Performance and Stability and Maneuverability*, Aviation Industry Press, Beijing, China, 1990.

[23] B. M. Kulfan, "Universal parametric geometry representation method," *Journal of Aircraft*, vol. 45, no. 1, pp. 142–158, 2008.

[24] M. Tahani, G. Kavari, M. Masdari, and M. Mirhosseini, "Aerodynamic design of horizontal axis wind turbine with innovative local linearization of chord and twist distributions," *Energy*, vol. 131, pp. 78–91, 2017.

[25] R. MacNeill and D. Verstraete, "Blade element momentum theory extended to model low Reynolds number propeller performance," *The Aeronautical Journal*, vol. 121, no. 1240, pp. 835–857, 2017.

[26] S. Lee, *Prediction of Acoustic Scattering in the Time Domain and Its Applications to Rotorcraft Noise*, The Pennsylvania State University, Pennsylvania State, PA, USA, 2009.

[27] A. Michaeli, "Equivalent edge currents for arbitrary aspects of observation," *IEEE Transactions on Antennas and Propagation*, vol. 32, no. 3, pp. 252–258, 1984.

[28] A. Bausssard, M. Rochdi, and A. Khenchaf, "PO/MEC-based scattering model for complex objects on a sea surface," *Progress in Electromagnetics Research*, vol. 111, pp. 229–251, 2011.

[29] M. Rochdi, A. Baussard, and A. Khenchaf, "PO/MEC-based bistatic scattering model for complex objects over a sea surface," in *Proceedings of the IEEE International Radar Conference (RADAR '10)*, pp. 993–998, Washington, DC, USA, May 2010.

[30] E. F. Knott, J. F. Shaeffer, and M. T. Tuley, *Radar Cross Section*, SciTech Publishing, Raleigh, NC, USA, 2nd edition, 2004.

[31] F. Farassat, "Derivation of formulations 1 and 1A of Farassat," NASA TM-2007-214853, 2007.

[32] Y. Liu, J. L. Jiao, C. Wang et al., *FEKO Simulation Principles and Engineering Applications*, Machinery Industry Press, Beijing, China, 2017.

[33] B. R. Jones, W. A. Crossley, and A. S. Lyrintzis, "Aerodynamic and aeroacoustic optimization of rotorcraft airfoils via a parallel genetic algorithm," *Journal of Aircraft*, vol. 37, no. 6, pp. 1088–1096, 2000.

[34] J. Lee and P. Hajela, "Parallel genetic algorithm implementation in multidisciplinary rotor blade design," *Journal of Aircraft*, vol. 33, no. 5, pp. 962–969, 1996.

[35] R. L. Haupt and S. E. Haupt, *Practical Genetic Algorithms*, John Wiley & Sons, Hoboken, NJ, USA, 2nd edition, 2004.